Heliyon 5 (2019) e02027

Contents lists available at ScienceDirect

Heliyon

journal homepage: www.heliyon.com

Facile one step synthesis method of spinel $LiMn_2O_4$ cathode material for lithium batteries

Ahmed M. Hashem [a,b,*], Somia M. Abbas [a], Xu Hou [b], Ali.E. Eid [a], Ashraf E. Abdel-Ghany [a]

[a] National Research Centre, Inorganic Chemistry Department, 33 El Bohouth St., (former El Tahrir St.), Dokki-Giza 12622, Egypt
[b] Helmholtz-Institute Münster, IEK-12, Forschungszentrum Jülich, GmbH, Münster, Germany

ARTICLE INFO

Keywords:
Electrochemistry
Inorganic chemistry
Materials chemistry
Physical chemistry
LIB
Cathode
LiMn2O4
Precipitation
Rate capability

ABSTRACT

This study succeeded to prepare three pure phases of Mn_2O_3, Mn_3O_4 beside one of the best cathode materials, spinel $LiMn_2O_4$. $LiMn_2O_4$ with high phase purity and crystallinity was synthesized by a facile, cost effective and one step synthesis method. The structure and morphology of the powders were studied in detail by means of X-ray diffraction (XRD), thermogravimetric analysis (TGA), field emission scanning electron microscopy (FESEM), transmission electron microscope (TEM) and surface area. The X-ray diffraction shows that the post-annealing process reveals the formation of pure crystalline spinel $LiMn_2O_4$ with small particle size and lower lattice strain. The thermogravimetric analysis threw the light on the role of the evaporation technique in producing $LiMn_2O_4$ by following the different phases on the thermal performance of the precursor. The morphological characterization shows the clear appearance of the octahedral particles of $LiMn_2O_4$ calcined at high temperature with microporous nanosized structure. Electrochemical testing of the as prepared spinel at 900 °C showed promising results in terms of high initial capacity and good cycle stability. The as prepared spinel sample shows also good rate performance.

1. Introduction

Continuous fluctuation of fossil fuel prices beside its depletion forced researchers to look for new energy resources. These trials to get clean energy can limit the emission of carbon dioxide which causes severe pollution. Solar and wind energy as sources for renewable energy sources go up and down with time and season of the year. As a result, the research focuses on the storage energy devices through energy conversion systems [1, 2]. Lithium-ion battery (LIB) is one of the most convenient energy storage system. LIB has high energy density and long service life for using in portable electronic devices e.g. cell phones, digital cameras and laptops. These kinds of batteries are using also in electric vehicles (EVs) and hybrid electric vehicles (HEVs). Such large applications need efficient cathode active materials with outstanding properties [3, 4]. One of these cathode materials is spinel lithium manganese oxide $LiMn_2O_4$(LMO) which is capable of replacing $LiCoO_2$. Spinel $LiMn_2O_4$on the contrary to $LiCoO_2$ is less expensive, more abundant and nontoxic. This material has also high energy density and thermal stability [5, 6, 7].

Last decade, $LiMn_2O_4$was prepared by different solid-state methods [8]. Although this method is one of the most scalable methods, it has many drawbacks. This method yields less homogenous large particle size materials as it requires that the mixed starting powders should be very well contacted [9]. Also solid state method requires high temperature to give the Li and Mn ions to form the spinel $LiMn_2O_4$ because some chemical bonds are broken and others are formed [10]. So spinel $LiMn_2O_4$ synthesized by this approach with good crystallinity can be obtained at 900 °C in air. However, some impurities such as Mn_3O_4 and Mn_2O_3 were also found in the final $LiMn_2O_4$ prepared by solid state reaction at 900 °C. These impurities affect negatively on its electrochemical properties in terms of the capacity fading at high temperature and/or at high current rate [11, 12]. To alleviate these drawbacks, soft wet chemical techniques have been used e.g. sol-gel method [13], combustion process [14], chemical precipitation [15] and hydrothermal method [16]. Navulla et al. [17] prepared a lithium-manganese cathode material by simple one-step solid-state reactions. Patey et al. [18] produced LMO nano particles by a one-step flame spray pyrolysis process. Bruce and co-workers [19] synthesized a stoichiometric LMO nanostructured cathode by a one-pot method. In this study we synthesize this material by facile one step synthesis method. To increase the charge – discharge rate and decrease the time of charging, synthesis of nanosized electrode materials by facile and efficient synthetic methods has taken special interest. It is a big challenge to synthesize good crystalline spinel $LiMn_2O_4$

* Corresponding author.
E-mail address: ahmedh242@yahoo.com (A.M. Hashem).

https://doi.org/10.1016/j.heliyon.2019.e02027
Received 10 February 2019; Received in revised form 20 May 2019; Accepted 28 June 2019

by complete one step method. The challenge is how to avoid the thermodynamic limitations that responsible for the conversion of Mn (IV) to Mn (III). Another challenge is how to alleviate the kinetic restrictions related to the inhomogeneous dispersion of reagents that leads to incomplete reaction. Impurities such as Mn_2O_3 and Mn_3O_4 cannot react with Li source to reconvert into $LiMn_2O_4$ because of insufficient thermal energy as the synthesis route adapts direct cooling step after calcination [20].

In this study, high performance spinel $LiMn_2O_4$ with good crystalline structure, rate performance and cycle stability was synthesized in a simple synthesis route (one step method). This method is facile, does not require expensive and sophisticated laboratory equipment and extraordinary experimental circumstances, therefore it is fairly financially savvy, as well as time consuming and easily scalable for mass production. The effect of the different calcination temperatures on the chemical and electrochemical properties of the spinel $LiMn_2O_4$ was investigated and discussed in details. Besides LMO materials, pure other manganese oxides such as. Mn_2O_3 and Mn_3O_4 were obtained also from this method. Other subsidiaries materials were obtained also as we will discuss in details.

2. Experimental

2.1. Synthesis of the samples

Spinel $LiMn_2O_4$ was prepared by one pot, one step, facile and cost effective method using evaporation technique. Stoichiometric amounts of lithium acetate (Analytical Rasayan.S.d.FINE-CHEM LTd) and manganese acetate (Sigma Aldrich) with molar ratio Li:Mn = 1:2 were dissolved and stirred in de-ionized water to form an aqueous solution and then immersed in cold water bath. Oxalic acid (Merck) as precipitating agent (molar ratio of oxalic acid: metal cations is 1:1) was added drop wisely to the above cold solution to precipitate mixture of manganese and lithium oxalate together. The entire solution was stirred at 80 °C to evaporate the water. After obtaining a viscous precipitation it was poured in a large petri dish to enhance the rate of evaporation in a wide area. We collected the precipitation and dried it at ca 80 °C overnight. The obtained dried and grounded powder was calcined in air at 450 °C and 750 °C for 5 h for each temperature and finally at 900 °C for 10 h with intermittent grinding. The final calcined samples were abbreviated as E450, E750 and E900.

The same procedure has been used as above mentioned with the same amounts of reagents. Instead of evaporating the solution directly, the precipitated precursor was filtrated in this case. The precipitate was collected and dried overnight then calcined under the same procedure at various temperatures 450 °C, 750 °C for 5 h for each temperature and finally at 900 °C for 10 h with intermittent grinding. The collected samples were named as F450, F750 and F900, respectively. The filtrate which was expected to be a salt of lithium was evaporated until dryness and labeled as LiR (dried at room temperature) and part of it was calcined at 450 °C for 5 h and labeled as Li450.

The main purpose of the second technique (filtration technique) is to confirm that the soluble lithium oxalate was penetrate through filtration process at room temperature as filtrate. After dryness, this filtrate has white color at room temperature and labeled as LiR (Fig. 1a) and it was mainly lithium hydrogen oxalate hydrate. After the calcination at 450 °C it converts to lithium carbonate and labeled as Li450 (Fig. 1b). The above filtrated powder has a pink color (Fig. 1c, labeled as FR) which favors the formation of manganese oxalate at room temperature and labeled as FR and turned to black after calcination at 450 °C and labeled as F450 (formation of manganese oxides as shown in Fig. 1d). On the contrary, in evaporation technique the calcined evaporated precursor at 450 °C which labeled as E450 has mixed colors of black (manganese oxide) and a light (lithium salt) as shown in Fig. (2a). Further calcination to 750 °C (E750) and 900 °C (E900) will lead to formation of spinel of black color (Figs.2b and 2c). As we above mentioned evaporation technique supports our intent to trap the lithium salt with the manganese salt in a

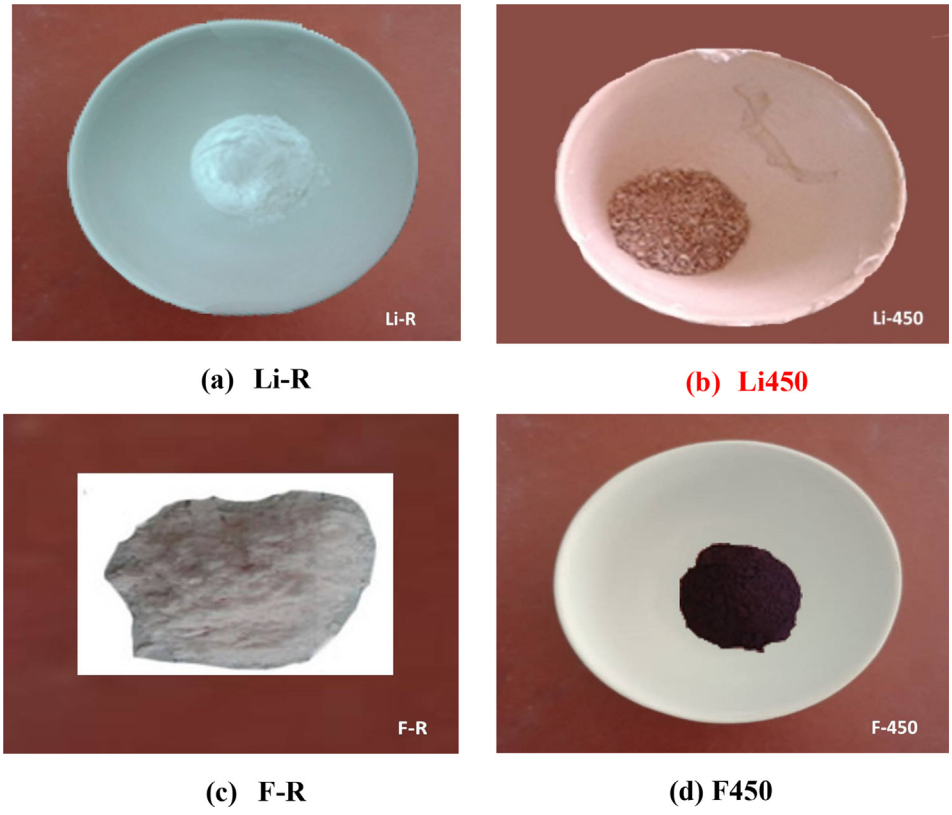

Fig. 1. Visual observation for the filtrate at a) room temperature and b) 450 °C and for the precipitate at c) room temperature and d) 450 °C produced from the filtration technique.

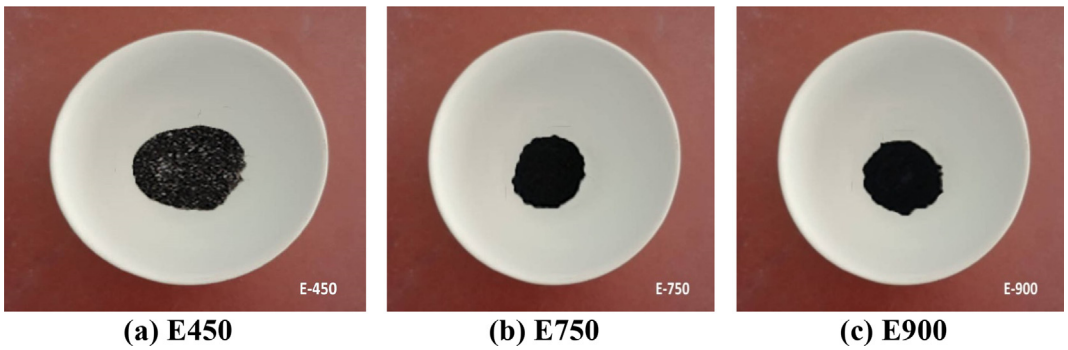

Fig. 2. Visual observation for the yields produced from evaporation technique and calcined at a) 450 °C, b) 750 °C and c) 900 °C.

homogenous mixture to obtain the pure spinel after further calcination at ca. 750 °C and/or 900 °C. This means just one step was used to obtain spinel instead of two steps in the traditional co precipitation method. In this traditional method manganese was precipitated first as hydroxide or oxalate then the precipitate was mixed with lithium salt by solid mixing which suffers from good homogeneity.

2.2. Characterization

The structure of the samples was analyzed by X-ray diffractometer (XRD) using a philipsX'Pert apparatus equipped with a CuKα X-ray source (λ = 1.54056Å). Data were collected in the 2θ range of 10–80°. TGA measurements were carried out using a thermal gravimetric analyzer (Perkin Elmer, TGA7 series) in the temperature range of 30-1000 °C in air at a heating rate of 10 °C/min. The surface morphology of the fabricated samples was visualized using a field emission scanning electron microscopy, (Quanta, FEG 250). The microstructure and morphology of the materials were observed with JEM-2100 (JEOL-ELECTRON MICROSCOPE). BET surface area and pore size distribution of synthesized samples were determined from N_2-adsorption experiments using (Belsorp max version 2.3.2).

Cathode materials for electrochemical testing were prepared by casting a slurry with a composition of 80 wt% $LiMn_2O_4$ active material, 10 wt% carbon black Super P or C65 (TIMCAL), and 10 wt% PVdF onto Al foil. Sheets of 12 mm circular pieces of positive electrode materials were used as working electrodes with mass loading area in the range 1.2–1.3 mg/cm^2. These cathode electrodes were assembled inside coin cells 2016-type with lithium metal foil as counter electrode and 1 M $LiPF_6$ in 1:1 ethylene carbonate: dimethyl carbonate (EC:DMC) as electrolyte. 0.1C was used as C-rate for cycling testing and 0.2 mV/S as scan rate for cyclic voltammetry testing. The cells were galvanostatically charged and discharged on Maccor series 4000 battery testers (USA) between 4.5 V and 3.5 V at 20 °C under different rates. The potentials reported in this work refer to the Li^+/Li couple.

3. Results and discussion

Fig. 3 shows the XRD pattern of $LiMn_2O_4$ synthesized by one step method using the evaporation technique and calcined at different temperatures. In Fig. 3(a) the pattern contains multiple phases of manganese oxides and lithium salt, which can later constitute the spinel $LiMn_2O_4$ at high temperature. By indexing the peaks, it is observed that these phases are $LiMn_2O_4$, MnO_2, Mn_2O_3 and Li_2CO_3. With rising the calcination temperature to 750 °C pure spinel $LiMn_2O_4$ is completely formed. Further rising to 900 °C confirms the formation of well crystalline pure spinel $LiMn_2O_4$ without appearing of any impurities as shown in Fig. 3(b, c). The complete formation of pure spinel $LiMn_2O_4$ at rather low temperature of 750 °C confirms that this method is feasible and effective due to the absence of impurities. This also means that calcination at 750 °C for 5 h looks a sufficient temperature with an appropriate time to burn off all

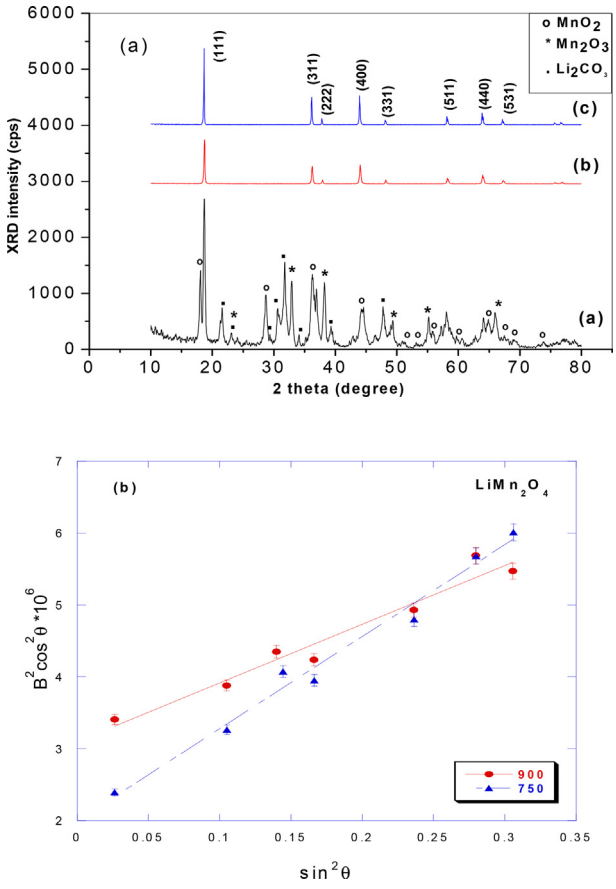

Fig. 3. [3a]. XRD patterns of sample (E) calcined at different temperatures (a) E450, (b) E750 (c) E900, and [3b] Analysis of the full width at half-maximum B of the Bragg reflections.

the organic materials used in the preparation in ambient atmosphere to form $LiMn_2O_4$ via one step method. Increasing annealing temperature 750 and 900 °C, the peaks are gradually sharpen which indicates an increase of crystallinity and the precursor are completely transformed into pure phase $LiMn_2O_4$ spinel powders without any development of minor phase. All the diffraction peaks could be indexed the cubic spinel structure with *Fd3m* space group (JCPDS No. 88-1749 card) [21]. As the calcinations temperature was getting higher, the main diffraction peaks of cubic spinel phase, such as (111), (311), and (400), were well developed. This means that lithium ions occupied tetrahedral 8*a* sites (Wyckoff notation) and manganese occupied octahedral 16*d* sites, while oxygen atoms are located at 32*e* sites [22]. The lattice parameters of $LiMn_2O_4$ calcined at 750 °C and 900 °C were calculated through the least square method using 10 well defined diffraction lines with indexation in

the cubic spinel structure and the results are listed in Table 1. The slight increasing in lattice parameter *a* upon rising the temperature is matched well with our previous work [22] and with result reported by Lee et al., [23]. To describe the variation of the crystallity size and quantify the local lattice strain of the two samples, Scherer's formula and the full width at maximum (FWHM) for different peaks especially (400) peak (because this peak is sensitive to calcinations temperature) are used, the data are summarized in Table 1. The domain size shows an increasing trend up to 900 °C, this indicates that the local field strain was decreased as a result of lattice ordering.

The FWHM values of the (311) and (400) diffraction lines of $LiMn_2O_4$ samples decrease with the increase of calcinations temperature (Table 1). This indicates that the spinel $LiMn_2O_4$ sample calcined at 900 °C might have higher crystallinity, better ordering of local structure, and lower lattice strain. Moreover, several authors reported that the ratio value of the $I_{(311)}/I_{(400)}$ peaks reflects the structural stability of the spinel structure by identifying the structural difference between lithium and manganese ions, i.e., some lithium and manganese ions are exchanged its location in spinel framework [24, 25, 26]. So that, the structural difference between the two samples may result from the different in calcinations temperature. Therefore, E900 synthesized at 900 °C has smaller $I_{(311)}/I_{(400)}$ ratio value than that of E750 synthesized at 750 °C, indicating that the confusion degree in E900 sample is smaller than that of E750 sample.

Fig. 4 represents the XRD pattern of the precipitation (FR) produced from the filtration technique, which is characterized to be manganese oxalate hydrate. All the diffraction peaks at ($2\theta = 18.43^{\circ}$, 18.8°, 22.63°, 24.47°, 29.78°, 33.34°, 33.7°, 39.26°, 42.02°, 44.34°, 47.38°, 49.34°) are indexed according to the monoclinic structure with *C2/c* space group [27] (JCPDS No. 25-0544 card). Then it has been calcined at different temperatures 450 °C, 750 °C and 900 °C respectively, and the XRD patterns are showed in Fig. 5. F450 is characterized as mixed phases of MnO_2 and Mn_2O_3. Rising the calcination temperature to 750 °C, the sample F750 shows the peaks at 23.15°, 32.8°, 38.2°, 45.1°, 49.22°, 55.25°, 65.81°. These peaks indexed very well to the phase of pure orthorhombic Mn_2O_3 with the corresponding miller indices ((211), (222), (400), (332), (431), (440), (622), respectively as in the (JCPDS Card data No. 24-0508) and are characteristic to Mn_2O_3 phase as reported by [28]. By further calcination at 900 °C, Mn_2O_3 was converted to pure tetragonal spinel Mn_3O_4 phase. Mn_3O_4 has the characteristic peaks located at ($2\theta = 18.7^{\circ}$, 28.9°, 32.344°, 36.14°, 38.03°, 44.41°, 50.75°, 58.51°, 59.9°, 64.7°) and matched with the miller indices (101), (112), (103), (211), (004), (220), (105), (321), (224), (400) as in (JCPDS: 24-0734) and as reported in literatures [29, 30].

Fig. 6 represents the XRD patterns of the filtrate precursor produced from the filtration technique at room temperature (LiR) and then calcined at 450 °C (Li450). Room temperature precursor is indexed as major phase of lithium hydrogen oxalate hydrate. With increasing temperature to 450 °C it converts to pure monoclinic Li_2CO_3. This pure phase matched very well with (JCPDS 87-0729) and with that reported by Yuan et al [31].

In conclusion filtration technique yields phases of manganese oxides produced from the precipitate and lithium salts produced from the soluble filtrate. On the contrary the evaporation technique succeeded to trap

Table 1
XRD data for $LiMn_2O_4$ synthesized by one step co-precipitation method using the evaporation technique and calcined at 750 °C and 900 °C.

E $LiMn_2O_4$	E 750 °C	E 900 °C
lattice parameters (Å)	8.226 (1)	8.231 (6)
unit cell volume ($Å^3$)	556.23	558.99
crystallite size (nm)	55.7	78.1
Strain $*10^{-4}$	8.9	6.8
FWHM (311)	0.243	0.168
FWHM (400)	0.253	0.186
I_{311}/I_{400}	0.972	0.950

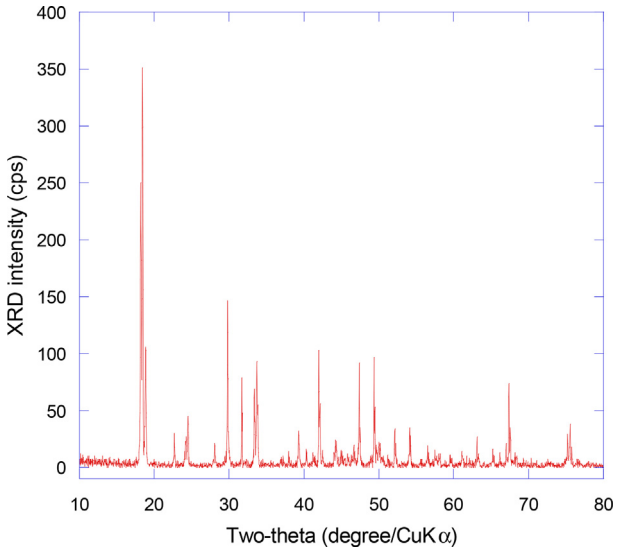

Fig. 4. XRD patterns of sample (F) at room temperature (FR).

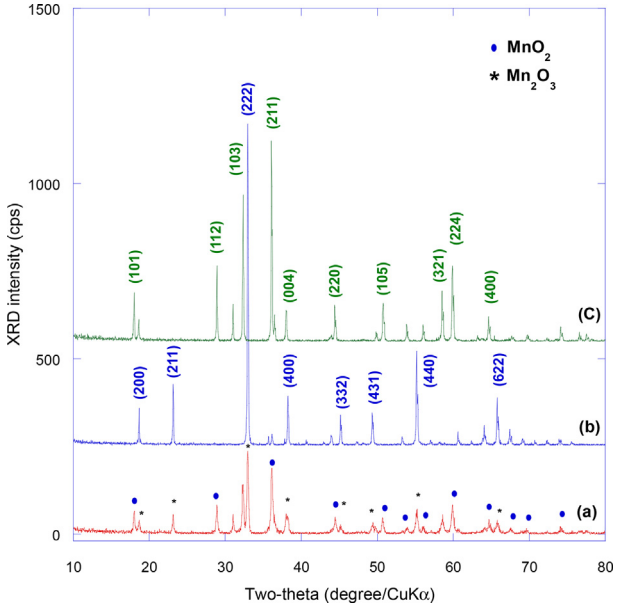

Fig. 5. XRD patterns of sample (F) calcined at different temperatures (a) F450 (MnO_2 and Mn_2O_3), (b) F750 (Mn_2O_3) (c) F900 (Mn_3O_4).

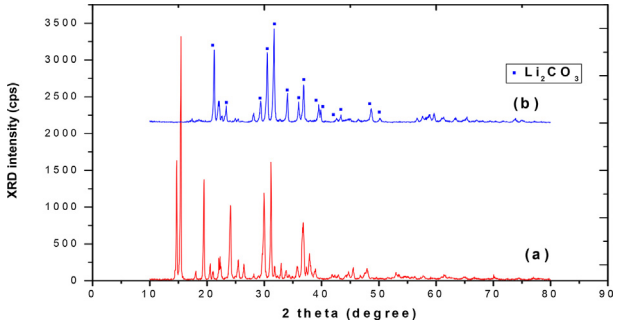

Fig. 6. XRD pattern of (a) LiR,(b) Li450.

soluble lithium reagent beside manganese reagent to yield the required $LiMn_2O_4$. This summation of the precipitate and the filtrate can be observed clearly from phases exist in the XRD pattern of sample E450 (MnO_2, Mn_2O_3 and Li_2CO_3). So we can say that the evaporation technique is one pot, one step and facile method to obtain pure spinel $LiMn_2O_4$. Instead of using less homogenous solid mixing of lithium salt with manganese salt to obtain pure spinel we succeeded to bring them together by this technique and increase the degree of homogeneity and hence get nanosize spinel $LiMn_2O_4$.

The thermal analysis is necessary to define the optimum heat-treated temperature required to determine the thermal behavior of the prepared samples. Thermal behavior of the precipitate precursor resulted from filtration technique and proved to be manganese oxalate hydrate by XRD (Fig. 4) is shown in Fig. 7. Pronounced weight loss observed at around 100 °C is ascribed to the dehydration of the precursor (hydrated manganese oxalate) and also to the evaporation of the free water adsorbed on the surface from the ambient atmosphere. Second remarkable weight loss recognized between100-140 °C is attributed to the loss of ≈14% related to water of crystallization or structure water accompanied by only one endothermic peak at 119.5 °C. Stable region is observed from 140 to about 265 °C which may represent formation of complete dehydrated manganese oxalate. Sudden and sharp weight loss of about 37% in the range from 250-350 °C is mainly attributed to the decomposition and evaporation of the organic constituents or oxalate of the precipitate accompanied by one exothermic peak at 304 °C. This thermal behavior is well agreed with the decomposition of the oxalate precursor reported before [27]. After this decomposition mixed phases from (MnO_2 and Mn_2O_3) was formed in the stable region from 340 to 440 °C and this is already observed from XRD mentioned above for sample F450 °C in Fig. 5a. The mixture started to decompose and reduce to pure Mn_2O_3 at about 470 °C. This oxygen loss of MnO_2 and formation of pure Mn_2O_3 agreed well with that reported in [32, 33] according to the following equation:

$$4MnO_2 = 2Mn_2O_3 + O_2$$

Mn_2O_3 still stable to nearly 885 °C and this stability was already confirmed from the XRD carried out for calcined sample at 750 °C (F750) displayed in Fig. 5b. Further reduction through loss of oxygen and formation of lower manganese oxide Mn_3O_4 was observed after 885 °C. This is also confirmed above in XRD Fig. 5c of sample F900 which calcined at 900 °C. Mn_3O_4 phase was observed clearly in this figure which confirms our interpretation and also supported by results from references [34, 35].

Fig. 8 shows the thermal behavior of the precursor resulted from evaporation technique. The behavior looks similar to that reported for

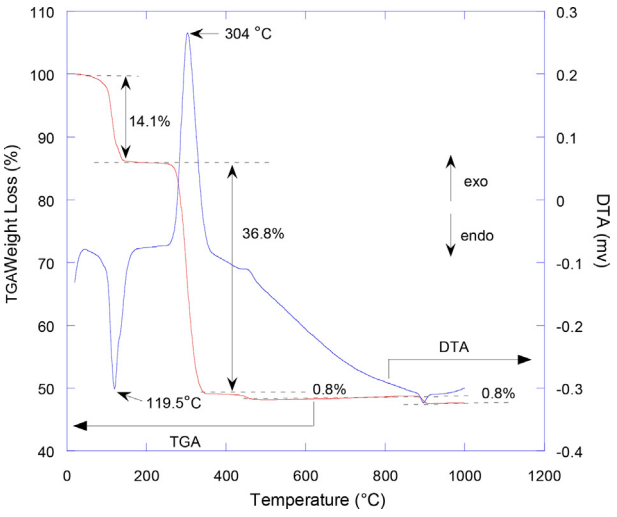

Fig. 7. TG/DTA of non - calcined precipitate of sample (F), from room temperature to 1000 °C using heating rate of 10 °C/min in air.

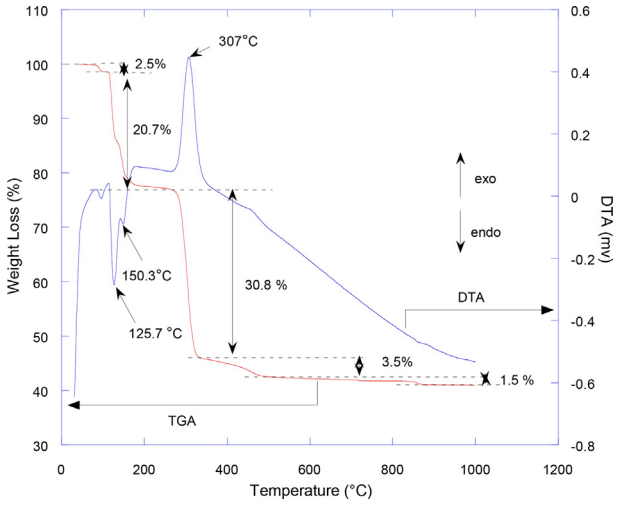

Fig. 8. TG/DTA of dried precipitate precursor of sample (E) from room temperature to 1000 °C using heating rate of 10 °C/min in air.

filtration technique in Fig. 7. Larger total weight loss of 23.2% observed in the region between 82-180 °C than that reported for sample (F) mentioned in Fig. 7 is attributed to loss of both water of hydration and water of constitution from mixed lithium hydrogen oxalate hydrate and hydrated manganese oxalate. This loss in water is confirmed from two successive endothermic peaks at 125.7 °C and 150.3 °C. The stable region between 180-270 °C may represent the formation of mixture of dehydrated manganese oxalate and lithium oxalate. Large weight loss of 30.8% observed in the region between 274-330 °C is due to decomposition of the organic constitute (oxalate) accompanied by sharp exothermic peak at 307 °C due to phase transition to mixture of some kinds of lithium and manganese oxides. After 330 °C there is an intermediate stage until formation of $LiMn_2O_4$ from association of MnO_2, Mn_2O_3 and Li_2CO_3 at 450 °C as illustrated above in XRD of sample E450. The transformation from lithium oxalate to lithium carbonate was confirmed before [36] to occur in the range of 400–500 °C. After this temperature combination between these three phases takes place to start to form pure spinel $LiMn_2O_4$ by the synergistic effect of the three components which still stable to more than 950 °C.

In Fig. 9 no distinct weight loss in the TGA curve of sample (E900) is observed which indicates that $LiMn_2O_4$ prepared by the one-step method using the evaporation technique has a stable structure and the small

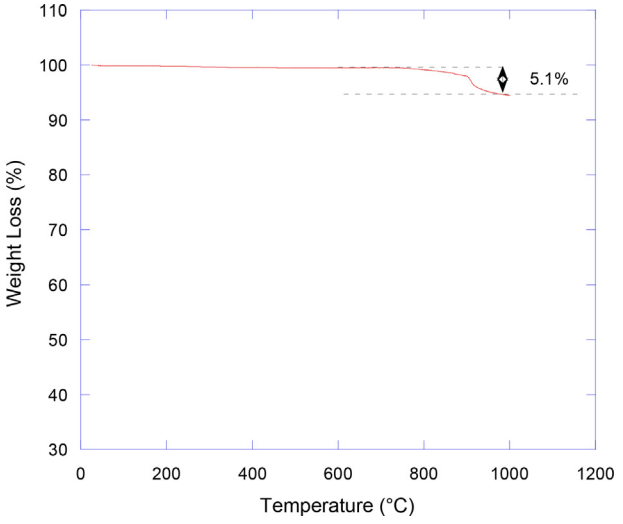

Fig. 9. TGA of spinel $LiMn_2O_4$ (sample E900) from room temperature to 1000 °C using heating rate of 10 °C/min in air.

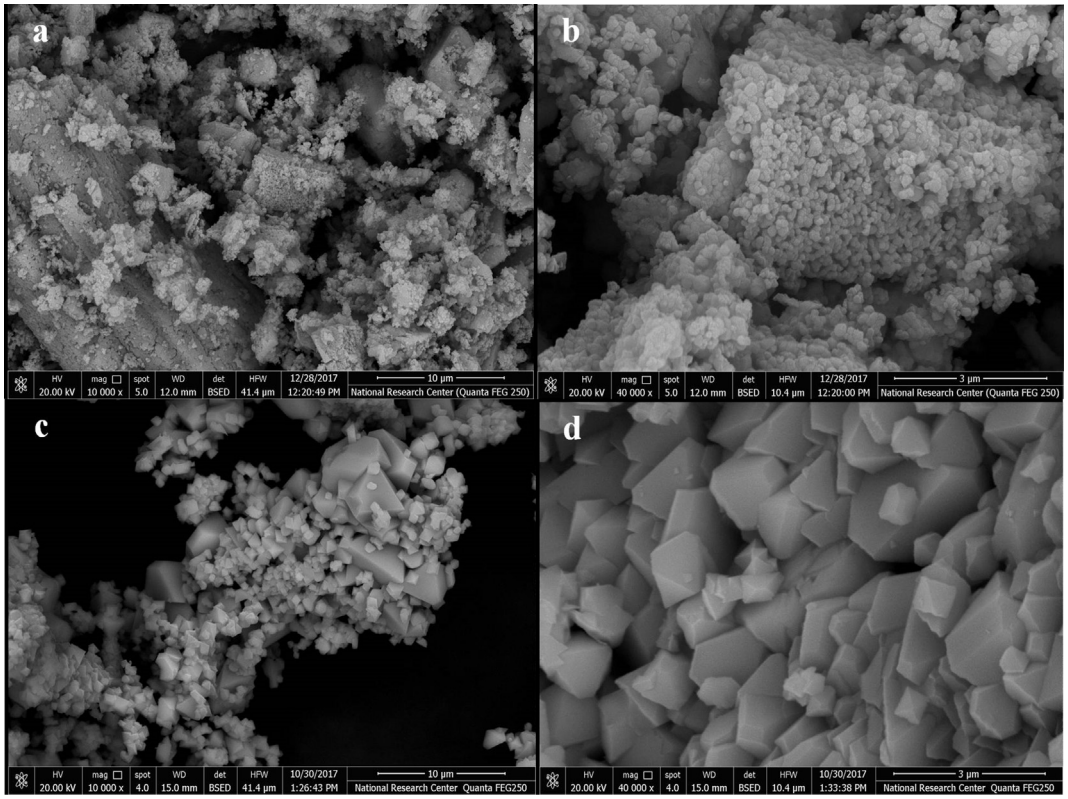

Fig. 10. FESEM of a,b) E750, (c,d) E900.

weight loss ≈5% that occurs above 900 °C may attribute to the volatilization and liberation of lithium at such high temperature.

It is known that the particle size and surface morphology can affect the electrochemical properties of the active electrode materials. Fig. 10 reveals the Field Emission Scanning Electron Microscope (FESEM) of $LiMn_2O_4$ samples calcined at different temperatures. It can be seen that the calcination temperature played an important role on the crystallinity of the material. The particle size increases with increasing sintering

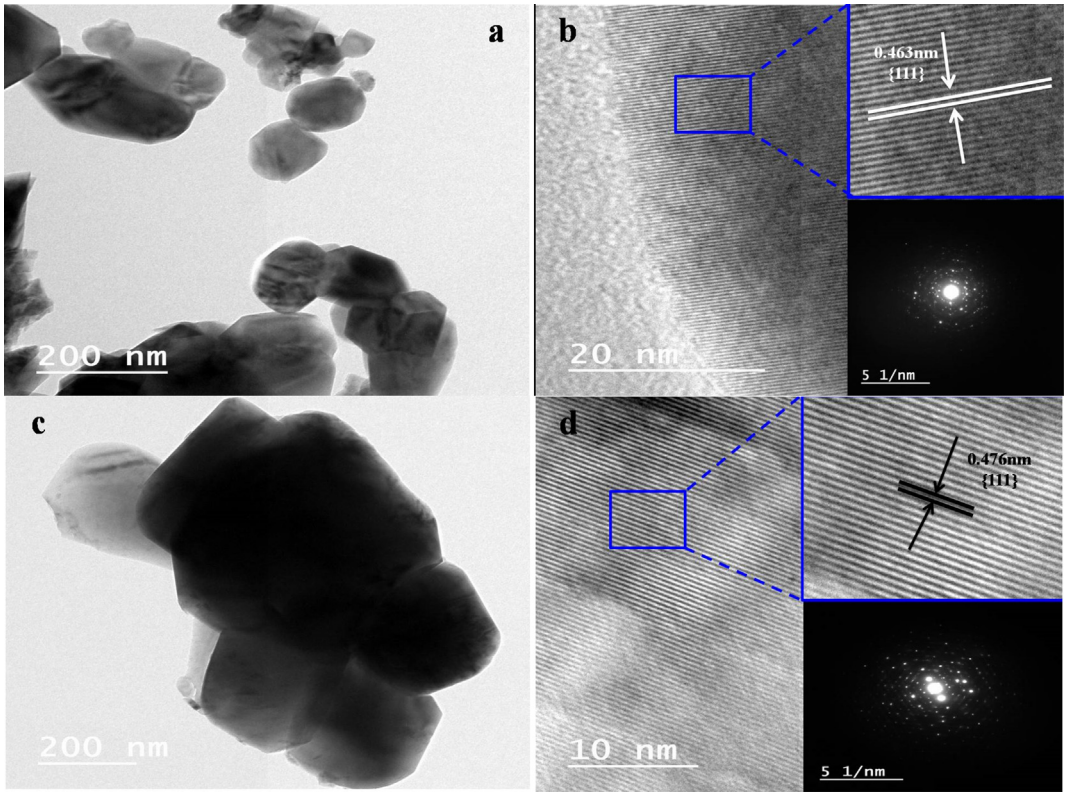

Fig. 11. TEM, HRTEM and SAED images for E750 (a, b), TEM, HRTEM and SAED images for E900 (c,d).

temperature. The average particle size of the samples calcined at 750 and 900 °C were found to be 100–200 and 200–500 nm, respectively. The samples calcined at 900 °C exhibits a more uniform particle size distribution and better crystallinity than the sample sintered at 750 °C. In addition, the images clearly visualizes the truncated surfaces at the vertices and edges of the parental octahedral structure, and the orientation of each surface was assigned following the established face orientation of the octahedral face-center cubic (fcc) framework, that is, {111}, as well as those of its truncated derivatives [37, 38, 39, 40].

The transmission electron microscopy (TEM) and selected area electron diffraction (SAED) are further utilized to give more detailed morphology and surface features of $LiMn_2O_4$. A typical TEM image of the selected random particle in $LiMn_2O_4$ samples as shown in Fig.11a and c, demonstrates that they have a truncated Oh crystal structure and their average particle size are 75–100 and 200–300nm for E750 and E900, respectively. To confirm the crystal structure of the prepared samples, HRTEM images and the corresponding selected area electron diffraction (SAED) patterns are shown in Fig. 11b,d for E750 and E900 respectively. In both samples, the apparent lattice fringes with interplanar distance of 0.463 and 0.476 nm for E750 and E900, respectively are clearly observed. These fringes are well assigned to the planar distance between (111) crystal faces of spinel $LiMn_2O_4$, indicating that the exposed planes are {111} facets. The electrode stability of $LiMn_2O_4$ depends on the reaction rate of SEI formation and the stability of the reconstructed surface structure, and {111} facets are more favorable in formation of allowable SEI on the surface of $LiMn_2O_4$ which facilitates Li^+ ions insertion/desertion. Therefore, we expected that the $LiMn_2O_4$ cathodes with exposed {111} facets could be used to provide better stability of the $LiMn_2O_4$ cathode against structural and volume change [41]. Moreover, the corresponding SAED patterns (inset of Fig. 11b and Fig. 11d) showed that a well-defined spots in two cathodes, while E900 have a well-defined spots rather than E750, implying that not only the two cathodes are in a single crystal structure but also the E900 cathode contain fewer defects and show higher structural stability than E750.

Fig. 12 displays the nitrogen adsorption–desorption isotherms and pore-size distributions (PSD) of E750 and E900 samples. According to IUPAC-classification, the isotherm curves and the hysteresis loop of $LiMn_2O_4$ calcined at both 750 °C and 900 °C belong to type IV with H3-hysteresis loop which implying the presence of porous structure [42, 43, 44]. Therefore, it can be concluded that the heat-treatment processes do not lead to a collapse of the mesostructure, which is also evidenced by the well-devolved TEM images. According to the pore size distribution of $LiMn_2O_4$ calcined at 750 °C and 900 °C, both two samples have microporous particles as estimated from PSD peaks centered at < 2 nm for both samples. These micropores act as channels for Li^+ ion diffusion as well as electrolyte penetration. Brunauer-Emmett-Teller (BET) specific surface area for $LiMn_2O_4$ calcined at 750 °C is 7.722 m^2g^{-1} which is larger by ten order of magnitude than that of E900 (0.68939 $m^2g^{-1)}$. So increasing calcination temperature to 900 °C increases the particle size as shown in TEM section and hence decreases the entire surface area as reported [45].

3.1. Electrochemical performance of $LiMn_2O_4$

As we mentioned above beside $LiMn_2O_4$ other two oxides of manganese oxides (Mn_2O_3 and Mn_3O_4) were obtained. These lower oxides have application also as anode active materials in lithium ion batteries as reported previously [46, 47]. The successful synthesis of pure $LiMn_2O_4$ in this study motivated us to investigate its electrochemical properties as cathode material in lithium ion batteries.

Fig. 13 represents the cyclic voltammograms behavior of spinel $LiMn_2O_4$ calcined at 900 °C (E900). There is no peak at 4.5 V which confirm that Mn is not present in the 8a tetrahedral sites (i.e; there is no cation mixing) [48]. Here in the figure we can observe two well-defined redox peaks, located at around 4.07/3.94V and 4.2/4.07V. These peaks indicate the reversible intercalation and de-intercalation processes of lithium-ions into this spinel structure. This means that lithium ions are

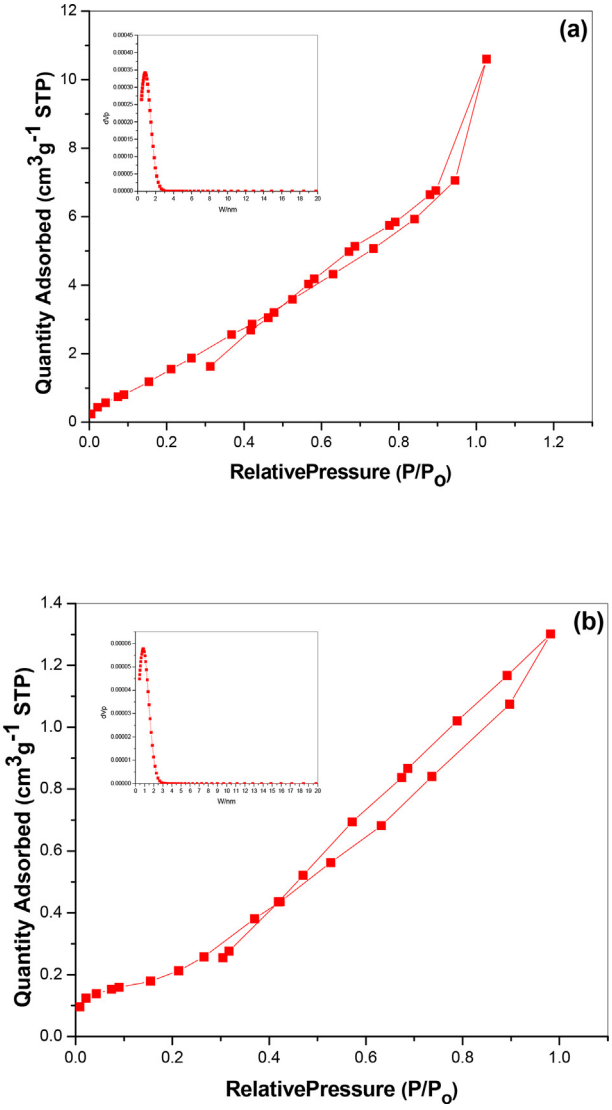

Fig. 12. Nitrogen adsorption/desorption isotherms for (a) E750, (b) E900. The insets are pore size distributions of the samples.

extracted and inserted into the spinel phase by a two-step process corresponding to $LiMn_2O_4/Li_{0.5}Mn_2O_4$ and $Li_{0.5}Mn_2O_4/\lambda$-MnO_2 during charging and vice versa during discharging [49]. It can be seen from the CV curves that the peaks become sharper and the splitting of the peaks becomes more well-defined (no overlapping) with decreasing in the potential difference upon cycling. This indicates the increase in the crystallinity of particles and hence the improvement of the reversibility due to the fast Li^+ ion transport.

Different C-rates were applied to test charge - discharge performance of $LiMn_2O_4$ with 3–4.5V potential range as shown in Fig. 14. From this figure we can notice that all charge-discharge profiles exhibit two obvious charge plateaus at 4.01 and 4.13 V and two obvious discharge plateaus at 4.099 V and 3.97. Theses redox plateaus agreed well with the redox peaks in CV analysis mentioned above and indicate good reversibility of spinel sample. By increasing the current to 5C, only a slope profile can be seen. this can be explained by rather increase in cell polarization at high current density.

This sample of spinel $LiMn_2O_4$ delivers an initial charge and discharge capacities of 129, 115 $mAhg^{-1}$ with a two-step potential profile. The coulombic efficiency is about 89.15% for the first cycle using 0.1C rate in the potential range of 3–4.5V. The efficiency increases with successive cycling and reached 100%. It is worth noting that the charge and

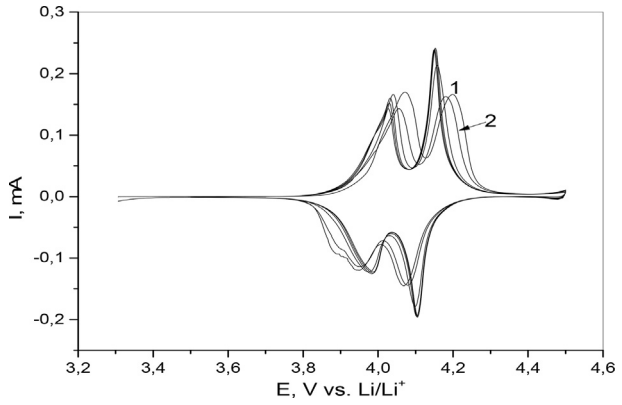

Fig. 13. Cyclic Voltammogram of $LiMn_2O_4$ (E900)cycled between 3.5 and 4.5 V (vs. Li^+/Li) at a scan rate of 0.02 mVs^{-1}.

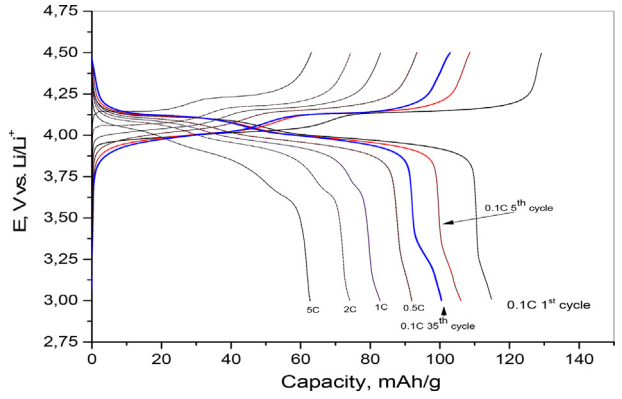

Fig. 14. Typical Galvanostatic charge–discharge curves for the $LiMn_2O_4$ sample (E900) at different C- rates within potential range 3–4.5V vs. Li/Li^+.

discharge capacities decrease with increasing the current density. The main reason for the gradual decrease in discharge capacity upon cycling in low or at different current densities is attributed to the structural change of spinel $LiMn_2O_4$ due to Jahn-Teller effect as ($2Mn^{3+}$ Mn^{2+} + Mn^{4+}) and the loss of active material with dissolution of Mn^{2+} into electrolyte [50, 51].

Fig. 15 Shows (charge/discharge) capacities vs. cycle number of $LiMn_2O_4$ at different current densities. The discharge capacities of $LiMn_2O_4$ at 0.1C, 0.5C, 1C, 2C, 5C and 10C are 115.2 mAh/g, 93 mAh/g, 82.6 mAh/g, 74.2 mAh/g, 62.8 mAh/g and 53.45 mAh/g, respectively. The cycling at the following C-rates 0.5C, 1C, 2C, 5C and 10C retained 80.73 %, 71.7%, 64.4%, 54.5%, 46.4%), respectively from the 1st discharge capacity mentioned for 0.1C. The decrease in the discharge capacity and capacity retention at high current rates is normal by the effect of cell polarization as discussed in the galvanostatic charge-discharge figure. When the current rate reverse back to 0.1C, the discharge capacity of $LiMn_2O_4$ is able to return about 104.8 mAh/g, capacity retention 90.97% of the initial capacity, indicating the reversibility of $LiMn_2O_4$. This rather good rate capability is may attribute to the stability of the stoichiometry and composition of structure of $LiMn_2O_4$ that improve the transfer of Li^+ ions.

Fig. 16 a and b show the cycling properties of $LiMn_2O_4$ at 0.1C within potential window 3–4.5V vs. Li/Li^+. The characteristic charge - discharge plateaus like mentioned above of spinel $LiMn_2O_4$ appear clearly. After 50th cycle the sample retained 76.4% discharge capacity from the 1st discharge capacity. It is well observed also that the columbic efficiency increased rapidly after two cycles and reached more than 99%.

The increase in columbic efficiency of $LiMn_2O_4$ with cycling could be due to reversible structural change during the lithium insertion/extraction processes as an indication of good rechargeability and

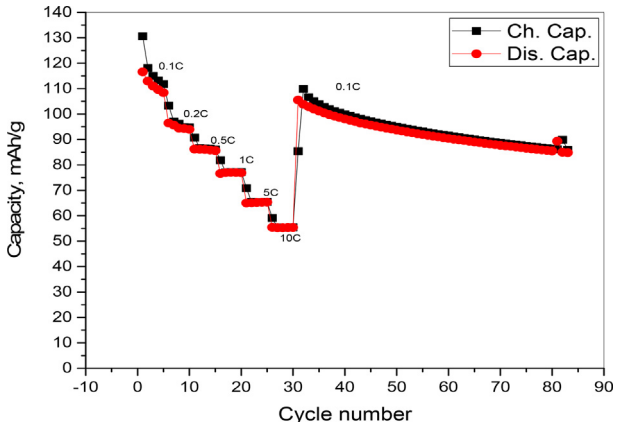

Fig. 15. Rate performance of the as prepared spinel $LiMn_2O_4$ at different current densities in the potential range 3–3.5V vs, Li/Li^+.

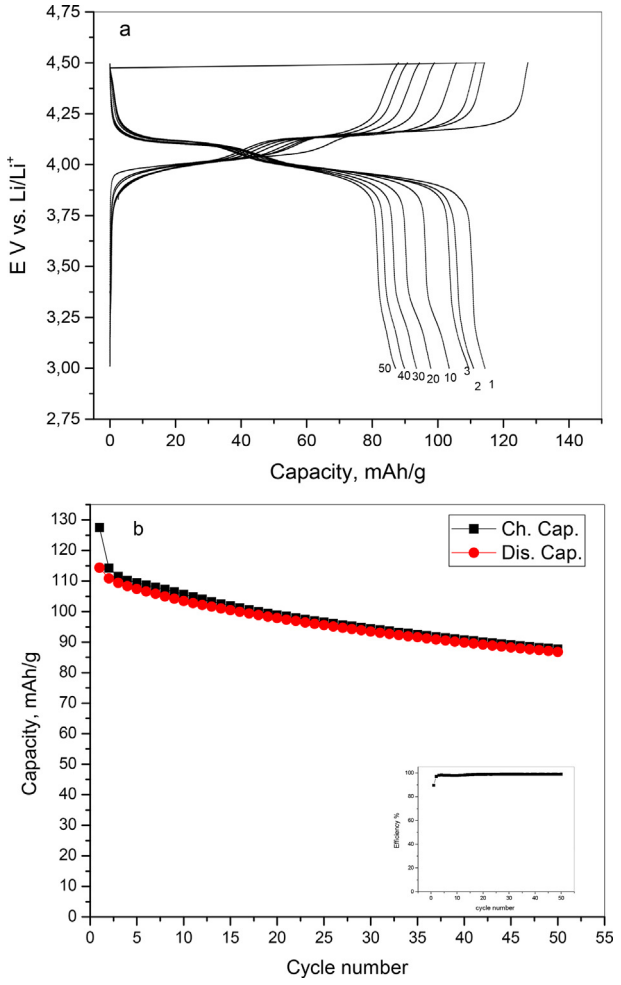

Fig. 16. a) charge/discharge cycles and b) capacity vs. cycle number with efficiency of $LiMn_2O_4$ at 0.1C within potential window 3–4.5V vs. Li/Li^+.

reversibility. The other reason could be the formation of stable electrode/electrolyte interface resulted from the higher oxidation state of the Mn ions (Mn^{4+}) which can provide rapid Li ions transportation [52]. The 100% coulombic efficiency and stability of charge/discharge capacities at high current rates indicate the stability of the structure and composition of the spinel $LiMn_2O_4$ with the intercalation/deintercalation of lithium.

4. Conclusion

The results reported in this study show that the strategy followed to prepare spinel $LiMn_2O_4$ material with high phase purity and crystallinity without any sophisticated equipment is a promising method. Other pure manganese suboxides e.g. Mn_2O_3 and Mn_3O_4 were obtained also in this study. Good morphological properties of as prepared $LiMn_2O_4$ improved its electrochemical properties as it significantly promotes fast insertion/extraction kinetics of lithium ions and facilitate charge transfer across the electrode/electrolyte interface reducing lithium ion diffusion length. This spinel delivered an initial discharge capacity of 115.2 mAh/g at 0.1C and a reversible discharge capacity of 104.8 mAh/g at the same rate with capacity retention of 90.97% after applying various C-rates. The charge and discharge capacities upon cycling and at high current rates are stable and reached to 100% coulombic efficiency. In summary, taking the facile synthesis method and the good microporous structure that lead to good electrochemical behavior into consideration, this porous $LiMn_2O_4$ material could be an attractive candidate for high energy/power lithium-ion batteries in future.

Declarations

Author contribution statement

Ahmed Hashem: Conceived and designed the experiments; Analyzed and interpreted the data; Wrote the paper.

Somia Abbas: Performed the experiments; Analyzed and interpreted the data; Wrote the paper.

Xu Hou: Contributed reagents, materials, analysis tools or data.

Ali Eid: Contributed reagents, materials, analysis tools or data; Wrote the paper.

Ashraf Abdel-Ghany: Conceived and designed the experiments; Analyzed and interpreted the data; Wrote the paper.

Funding statement

Ahmed M Hashem was supported by the Science and Technology Development Fund (STDF) through the project number 23159 (Economical synthesis methods for nanosized energy storage cathode materials to be used in lithium-ion batteries).

Competing interest statement

The authors declare no conflict of interest.

Additional information

No additional information is available for this paper.

References

[1] H. Xia, Z.J. Xie, Nanostructured $LiMn_2O_4$ and their composites as high-performance cathodes for lithium-ion batteries, Prog. Nat. Sci. Mater. Int. 22 (6) (2012) 572–584.

[2] W. Tang, L.L. Liu, S. Tian, L. Li, L.L. Li, Y.B. Yue, Y. Bai, Y.P. Wu, K. Zhu, R. Holze, $LiMn_2O_4$nanorods as a super-fast cathode material for aqueous rechargeable lithium batteries, Electrochem. Commun. 13 (2011) 1159–1162.

[3] J.B. Goodenough, Y. Kim, Challenges for rechargeable Li batteries, Chem. Mater. 22 (2010) 587–603.

[4] Z. Li, J. Zhang, J. Shu, J. Chen, C. Gong, J. Guo, L. Yu, J. Zhang, Carbon nanofibers with highly dispersed tin and tin antimonide nanoparticles: preparation via electrospinning and application as the anode materials for lithium-ion batteries, J. Power Sources 381 (2018) 1–7.

[5] K. Zhang, X.P. Han, Z. Hu, X.L. Zhang, Z.L. Tao, J. Chen, Nanostructured Mn-based oxides for electrochemical energy storage and conversion, Chem. Soc. Rev. 44 (2015) 699–728.

[6] S. Myung, K. Amine, Y. Sun, Nanostructured cathode materials for rechargeable lithium batteries, J. Power Sources 283 (2015) 219–236.

[7] F.X. Mao, W. Guo, J.M. Ma, Research progress on design strategies, synthesis and performance of $LiMn_2O_4$-based cathodes, RSC Adv. 5 (2015) 105248–105258.

[8] J.-H. Choy, D.-H. Kim, C.-W. Kwon, S.-J. Hwang, Y.-I. Kim, Physical and electrochemical characterization of nanocrystalline $LiMn_2O_4$ prepared by a modified citrate route, J. Power Sources 77 (1999) 1–11.

[9] Y. Xia, M. Yoshio, Studies on Li-Mn-O spinel system (obtained from melt-impregnation method) as a cathode for 4 V lithium batteries, part II. Optimum spinel from γ-MnOOH, J. Power Sources 57 (1995) 125–131.

[10] A.R. West, Solid State Chemistry and its Application, John wiley and Sons, U.S., 1984.

[11] J. Darul, W. Nowicki, C. Lathe, P. Piszora, Observation of phase transformations in $LiMn_2O_4$ under high pressure and at high temperature by in situ X-ray diffraction measurements, Radiat. Phys. Chem. 80 (2011) 1014–1018.

[12] K.S. Lee, S.T. Myung, H.G. Jung, J.K. Lee, Y.-K. Sun, Spinel lithium manganese oxide synthesized under a pressurized oxygen atmosphere, Electrochim. Acta 55 (2010) 8397–8401.

[13] M. Michalska, L. Lipińska, M. Mirkowska, M. Aksienionek, R. Diduszko, M. Wasiucionek, Nanocrystalline lithium–manganese oxide spinels for Li-ion batteries — sol-gel synthesis and characterization of their structure and selected physical properties Solid State Ion 188 (2011) 160–164.

[14] C.-Z. Lu, T.-K. Fey, Nanocrystalline and long cycling $LiMn_2O_4$ cathode material derived by a solution combustion method for lithium ion batteries, J. Phys. Chem. Solids 67 (2006) 756–761.

[15] A.R. Naghash, J.Y. Lee, Preparation of spinel lithium manganese oxide by aqueous co-precipitation, J. Power Sources 85 (2000) 284–293.

[16] R. Jiang, C. Cui, H. Ma, Poly (vinyl pyrrolidone)-assisted hydrothermal synthesis of $LiMn_2O_4$ nanoparticles with excellent rate performance, Mater. Lett. 91 (2013) 12–15.

[17] A. Navulla, L. Huynh, Z. Wei, A.S. Filatov, E.V. Dikarev, Volatile single-source molecular precursor for the lithium ion battery cathode, J. Am. Chem. Soc. 134 (2012) 5762–5765.

[18] T.J. Patey, R. Büchel, M. Nakayama, P. Novák, Electrochemistry of $LiMn_2O_4$ nanoparticles made by flame spray pyrolysis, Phys. Chem. Chem. Phys. 11 (2009) 3756–3761.

[19] K.M. Shaju, P.G. Bruce, A stoichiometric Nano-$LiMn_2O_4$ spinel electrode exhibiting high power and stable cycling, Chem. Mater. 20 (2008) 5557–5562.

[20] J. Yao, C. Shen, P. Zhang, D.H. Gregory, L. Wang, Enhanced cycleability of spinel $LiMn_2O_4$ by controlling the phase purity and structural strain, J. Phys. Chem. Solids 73 (2012) 1390–1395.

[21] K. Hariprasad, N. Naresh, B.N. Rao, M. Venkateswarlu, N. Satyanarayana, Preparation of $LiMn_2O_4$ nanorods and nanoparticles for lithium-ion battery applications, Mater. Today: Proc. 3 (2016) 4040–4045.

[22] A.M. Hashem, A.E. Abdel-Ghany, H.M. Abuzeid, R.S. El-Tawil, S. Indris, H. Ehrenberg, A. Mauger, C.M. Julien, EDTA as chelating agent for sol-gel synthesis of spinel $LiMn_2O_4$cathode material for lithium batteries, J. Alloy. Comp. 737 (2018) 758–766.

[23] Y. Lee, Y.K. Sun, K.S. Nahm, Synthesis of spinel $LiMn_2O_4$ cathode material prepared by an adipic acid-assisted sol–gel method for lithium secondary batteries, Solid State Ionics 109 (1998) 285–294.

[24] M.M. Thackeray, Manganese oxides for lithium batteries, Prog. Solid State Chem. 25 (1997) 1–71.

[25] Y.U. Ze-inin, ZHAO Lian-cheng, Structure and electrochemical properties of $LiMn_20_4$, Trans. Nonferrous Metals Soc. China 17 (2007) 659–664.

[26] S.-J. Bao, C.-M. Li, H.-L. Li, J.H.T. Luong, Morphology and electrochemistry of $LiMn_2O_4$ optimized by using different Mn-sources, J. Power Sources 164 (2007) 885–889.

[27] F. Davar, F. Mohandes, M. Salavati-Niasari, Synthesis and characterization manganese oxide nanobundles from decomposition of manganese oxalate, Inorg. Chim. Acta 362 (2009) 3663–3668.

[28] Y. Fang, Y. Huang, S. Zhang, W. Jia, X. Wang, Y. Guo, D. Jia, L. Wang, Synthesis of unique hierarchical mesoporous layered-cube Mn_2O_3 by dual-solvent for high-capacity anode material of lithium-ion batteries, Chem. Eng. J. 315 (2017) 583–590.

[29] J. Hao, J. Mou, J. Zhang, L. Dong, W. Liu, C. Xu, F. Kang, Electrochemically induced spinel-layered phase transition of Mn_3O_4 in high performance neutral aqueous rechargeable zinc battery, Electrochim. Acta 259 (2018) 170–178.

[30] S.-H. Park, W.-J. Lee, Hierarchically mesoporous carbon nanofiber/Mn_3O_4coaxial nanocables as anodes in lithium ion batteries, J. Power Sources 281 (2015) 301–309.

[31] B. Yuan, J. Wang, W. Cai, Y. Yang, M. Yi, L. Xiang, Effects of temperature on conversion of Li_2CO_3 to LiOH in $Ca(OH)_2$ suspension, Particuology 34 (2017) 97–102.

[32] J. Lu, C. Zhou, Z. Liu, K.S. Lee, L. Lu, $LiMn_2O_4$ cathode materials with large porous structure and radial interior channels for lithium ion batteries, Electrochim. Acta 212 (2016) 553–560.

[33] A.M. Hashem, A.E. Abdel-Ghany, R. El-Tawil, A. Bhaskar, B. Hunzinger, H. Ehrenberg, A. Mauger, C.M. Julien, Urchin-like α-MnO_2 formed of nanoneedles for high-performance lithium batteries, Ionics 22 (2016) 2263–2271.

[34] E.D. Mackien, Influence of atmosphere on the thermal decomposition of some transition metal oxalates, J. Inorg. Nucl. Chem. 30 (1968) 2689–2695.

[35] S. Singh, M. Chawla, P.F. Siril, G. Singh, Manganese oxalate nanorods as ballistic modifier for composite solid propellants, Thermochim. Acta 597 (2014) 85–92.

[36] M.M. Girgis, A.M. El-Awad, Kinetics and mechanism of thermal decomposition of lithium oxalate catalyzed by $Cd_{1-x}CoFe_2O_4$ (X = 0.0, 0.5 and 1.0) ferrospinel additives, Thermochim. Acta 214 (1993) 291–303.

[37] C. Yang, Y. Deng, M. Gao, X. Yang, X. Qin, G. Chen, High-rate and long-life performance of a truncated spinel cathode material with off-stoichiometric composition at elevated temperature, Electrochim. Acta 225 (2017) 198–206.

[38] L. Duan, X. Zhang, K. Yue, Y. Wu, J. Zhuang, W. Lü, Synthesis and electrochemical property of $LiMn_2O_4$ porous hollow nanofiber as cathode for lithium-ion batteries, Nanoscale Res. Letters 12 (2017) 109.
[39] Y.L. Ding, X.B. Zhao, J. Xie, G.S. Cao, T.J. Zhu, H.M. Yu, C.Y. Sun, Double-shelled hollow microspheres of $LiMn_2O_4$ for high-performance lithium ion batteries, Mater. Chem. 21 (2011) 9475–9479.
[40] Q. Li, J. Zhang, C. Gong, J. Guo, L. Yu, J. Zhang, Spinel $LiMn_2O_4$ cathode materials for lithium storage: the regulation of exposed facets and surface coating, Ceram. Int. 45 (2019) 13198–13202.
[41] J.-S. Kim, K.S. Kim, W. Cho, W.H. Shin, R. Kanno, J.W. Choi, A truncated manganese spinel cathode for excellent power and lifetime in lithium-ion batteries, Nano Lett. 12 (2012) 6358–6365.
[42] J.-Y. Luo, Y. Wang, H.-M. Xiong, Y.-Y. Xia, Ordered mesoporous spinel $LiMn_2O_4$ by a soft-chemical process as a cathode material for lithium-ion batteries, Chem. Mater. 19 (2007) 4791–4795.
[43] S.J. Gregg, K.S.W. Sing, Adsorption, Surface Area and Porosity, second ed., Academic Press, London, 1982.
[44] Z. Li, Q. Yin, W. Hu, J. Zhang, J. Guo, J. Chen, T. Sun, C. Du, J.L. Yu, J. Zhang, Tin/tin antimonide alloy nanoparticles embedded in electrospun porous carbon fibers as anode materials for lithium-ion batteries, J. Mater. Sci. 54 (2019) 9025–9033.
[45] Z. Zou, Z. Li, H. Zhang, X. Wang, C. Jiang, Copolymerization-assisted preparation of porous $LiMn_2O_4$ hollow microspheres as high power cathode of lithium-ion batteries, J. Mater. Sci. Technol. 33 (2017) 781–787.
[46] J. Yue, X. Gu, L. Chen, N. Wang, X. Jiang, H. Xu, J. Yang, Y. Qian, General synthesis of hollow MnO_2, Mn_3O_4 and MnO nanospheres as superior anode materials forlithium ion batteries, J. Mater. Chem. A 2 (2014) 17421–17426.
[47] D. Zhang, G. Li, J. Fan, B. Li, L. Li, In Situ synthesis of Mn_3O_4 nanoparticles on hollow carbon nanofiber as high-performance lithium-ion battery anode, Chem. Eur J. 24 (2018) 1–8.
[48] J.M. Tarascon, W.R. McKinnon, F. Coowar, T.N. Bowmer, G. Amatucci, D. Guyomard, Synthesis conditions and oxygen stoichiometry effects on Li insertion into the spinel $LiMn_2O_4$, J. Electrochem. Soc. 141 (1994) 1421–1431.
[49] Y. Xia, M. Yoshio, An investigation of lithium ion insertion into spinel structure Li-Mn-O compounds, J. Electrochem. Soc. 143 (1996) 825–833.
[50] D.K. Kim, P. Muralidharan, H.W. Lee, R. Ruffo, Y. Yang, C.K. Chan, H.L. Peng, R.A. Huggins, Y. Cui, Spinel $LiMn_2O_4$ nanorods as lithium ion battery cathodes, Nano Lett. 8 (2008) 3948–3952.
[51] M. Wakihara, H. Ikuta, Y. Uchimoto, Structural stability in partially substituted lithium manganese spinel oxide cathode, Ionics 8 (2002) 329–338.
[52] J. Yao, C. Shen, P. Zhang, D.H. Gregory, L. Wang, Enhanced cycleability of spinel $LiMn_2O_4$ by controlling the phase purity and structural strain, J. Phys. Chem. Solids 73 (2012) 1390–1395.